


RESEARCH ARTICLE

Organ-level right ventricular dysfunction with preserved Frank-Starling mechanism in a mouse model of pulmonary arterial hypertension

 Zhijie Wang,^{1,4} Jitandrakumar R. Patel,² David A. Schreier,¹ Timothy A. Hacker,³ Richard L. Moss,² and Naomi C. Chesler^{1,3}

¹Department of Biomedical Engineering, University of Wisconsin-Madison, Madison, Wisconsin; ²Department of Cell and Regenerative Biology, University of Wisconsin-Madison, Madison, Wisconsin; ³Department of Medicine, University of Wisconsin-Madison, Madison, Wisconsin; and ⁴Department of Mechanical Engineering, Colorado State University, Fort Collins, Colorado

Submitted 9 August 2017; accepted in final form 22 January 2018

Wang Z, Patel JR, Schreier DA, Hacker TA, Moss RL, Chesler NC. Organ-level right ventricular dysfunction with preserved Frank-Starling mechanism in a mouse model of pulmonary arterial hypertension. *J Appl Physiol* 124: 1244–1253, 2018. First published January 25, 2018; doi:10.1152/jappphysiol.00725.2017.—Pulmonary arterial hypertension (PAH) is a rapidly fatal disease in which mortality is due to right ventricular (RV) failure. It is unclear whether RV dysfunction initiates at the organ level or the subcellular level or both. We hypothesized that chronic pressure overload-induced RV dysfunction begins at the organ level with preserved Frank-Starling mechanism in myocytes. To test this hypothesis, we induced PAH with Sugren + hypoxia (HySu) in mice and measured RV whole organ and subcellular functional changes by *in vivo* pressure-volume measurements and *in vitro* trabeculae length-tension measurements, respectively, at multiple time points for up to 56 days. We observed progressive changes in RV function at the organ level: in contrast to early PAH (14-day HySu), in late PAH (56-day HySu) ejection fraction and ventricular-vascular coupling were decreased. At the subcellular level, direct measurements of myofilament contraction showed that RV contractile force was similarly increased at any stage of PAH development. Moreover, cross-bridge kinetics were not changed and length dependence of force development (Frank-Starling relation) were not different from baseline in any PAH group. Histological examinations confirmed increased cardiomyocyte cross-sectional area and decreased von Willebrand factor expression in RVs with PAH. In summary, RV dysfunction developed at the organ level with preserved Frank-Starling mechanism in myofilaments, and these results provide novel insight into the development of RV dysfunction, which is critical to understanding the mechanisms of RV failure.

NEW & NOTEWORTHY A multiscale investigation of pulmonary artery pressure overload in mice showed time-dependent organ-level right ventricular (RV) dysfunction with preserved Frank-Starling relations in myofilaments. Our findings provide novel insight into the development of RV dysfunction, which is critical to understanding mechanisms of RV failure.

hypertrophy; myocyte morphology; right heart failure; skinned trabeculae; ventricular-vascular coupling

INTRODUCTION

Pulmonary hypertension (PH) is a complex disorder that manifests as abnormally high blood pressure in the pulmonary vasculature. The World Health Organization (WHO) has classified the disease into five categories: Group I, pulmonary arterial hypertension (PAH) resulting from increased pulmonary vascular resistance; Group II, PH associated with left heart disease; Group III, PH associated with lung diseases and/or hypoxemia; Group IV, PH due to chronic thrombotic and/or embolic disease; and Group V, other miscellaneous causes (29). PAH is the most severe form of PH due to its rapid progression to right ventricular failure (RVF) (48). In the lungs, it is manifested as marked arterial remodeling and occlusion, mostly at the small distal arterioles, as well as mechanical stiffening of both proximal and distal pulmonary arteries (50). Left untreated, the estimated median survival of PAH is 2.8 years (17). Treatment strategies for PAH focus on reversing or reducing pulmonary vascular remodeling. However, even with modern therapy, PAH patients eventually develop RVF and the clinical outcomes are poor (47, 48). The mechanisms that underlie RV dysfunction and failure remain poorly understood.

A variety of tools have been developed to measure ventricular function at different scales (i.e., from the organ level to the subcellular level). The gold standard for assessment of ventricular performance at the organ level is *in vivo* pressure-volume (PV) measurement, which has been performed in the RV of patients (22, 31) and of rodent models of disease (1–3, 7, 41). At the cellular or subcellular level, a common approach for studying ventricular biomechanical performance is via length-tension relationships of isolated myocytes or trabeculae. This approach has been used in a limited number of studies investigating RV functional changes in response to PAH in human subjects (36), neonatal calves (49), and rats (8, 23, 35). Although these reports provide pioneering data about the changes in RV myofilaments in response to pressure overload, discrepant findings have been published such as the changes in Ca²⁺ sensitivity of myocardial force: a decrease in Ca²⁺ sensitivity is found in hypoxic neonatal calves RVs (49) whereas no change in Ca²⁺ sensitivity is reported by others in PAH patient RVs or rat RVs (8, 23, 36).

Moreover, none of the previous studies have investigated temporal changes in RV function due to chronic pressure

Address for reprint requests and other correspondence: N. C. Chesler, 2146 Engineering Centers Building, 1550 Engineering Dr., Madison, WI 53706 (e-mail: naomi.chesler@wisc.edu).

overload at both the organ level and the subcellular level. Therefore, it is unknown whether RV impairment originates at the organ level or the subcellular level or both simultaneously, leading to limited insight into the mechanisms of RV failure.

In the present study, we hypothesized that chronic pressure overload due to PAH initiates RV dysfunction at the organ level with preserved Frank-Starling mechanism in myofilaments. To test this hypothesis, we adapted a recently established mouse PAH model, by which PAH is induced by the combined exposure to chronic hypoxia and weekly injection of Sugen (HySu), a vascular endothelial growth factor (VEGF) receptor inhibitor (4). We extended the HySu treatment from 2 wk to 8 wk and then characterized RV function at both whole organ and subcellular levels at different time points. Cellular and molecular changes in RVs were examined by histology and immunohistochemistry. Our main finding is that chronic pressure overload caused RV dysfunction at the organ level with preserved Frank-Starling relations at the subcellular level.

MATERIALS AND METHODS

Animal preparation for in vivo hemodynamic measurements. Male C57BL6/J mice were obtained from Jackson Laboratory (Bar Harbor, ME); female mice were not used to reduce variability due to sex differences (26). Mice were assigned into one of four groups for exposure to 0 ($N = 9$), 14 ($N = 9$), 28 ($N = 8$), or 56 ($N = 8$) days of normobaric hypoxia (10% oxygen); animals exposed to hypoxia were also treated weekly with Sugen (SU5416, Sigma) at a dose of 20 mg/kg via intraperitoneal (ip) injection. The 0-day, normoxia control group was housed in room air; these animals were treated weekly with ($N = 5$) or without ($N = 4$) vehicle [i.e., carboxymethyl cellulose sodium (CMC) solution: 0.5% (wt/vol) CMC, 0.9% (wt/vol) sodium chloride, 0.4% (vol/vol) polysorbate 80, 0.9% (vol/vol) benzyl alcohol in deionized water] for 3 wk. We did not observe any differences between the nontreated and 3-wk CMC-treated controls. All mice were 10–14 wk of age at the time of euthanasia to minimize the effects of aging. As a consequence, mice were 6 wk old at the start of the 56-day exposure, 8 wk old at the start of the other HySu exposures, and 10 wk old at the start of the normoxic (control) exposures. The University of Wisconsin Institutional Animal Care and Use Committee approved all procedures.

Anesthesia, ventilation, and ventricular exposure. For in vivo pressure-volume (PV) measurements, mice were anesthetized with urethane solution (1,000–1,200 mg/kg body wt ip), intubated, and placed on a ventilator (Harvard Apparatus, Holliston, MA) using a tidal volume of ~ 225 μ l room air at a respiratory rate of ~ 125 breaths/min. They were then placed supine on a heated pad to maintain body temperature at 38–39°C. A ventral midline skin incision was made and the thoracic cavity was entered through the sternum. The chest wall and lungs were carefully retracted to expose the RV. Hydroxyethylstarch (~ 24 μ g) (6%; 2 mg/g body wt) was injected intravenously to restore vascular volumes (39).

Instrumentation and in vivo hemodynamic measurements. The left carotid artery was cannulated with a 1.2-F catheter with a pressure transducer at the tip (Scisense, London, Ontario, Canada) and advanced into the ascending aorta to measure systemic blood pressure. Subsequently, the RV apex was localized and a 1.2-F admittance pressure-volume (PV) catheter (Scisense) was introduced using a 20-gauge needle leaving the pericardium intact. After instrumentation was established and initial PV measurements were obtained, the inferior vena cava was isolated and briefly occluded to obtain alterations in venous return for determination of end-systolic PV relations (i.e., ESPVR). This vena cava occlusion (VCO) was limited to a few seconds in duration to avoid reflex responses. VCO was performed at least three times. The magnitude and phase of the electrical admit-

tance as well as the RV pressure were continuously recorded at 1,000 Hz and analyzed on commercially available software (Notocord Systems, Croissy Sur Seine, France) as previously reported (39, 41).

After the in vivo measurements, animals were euthanized by exsanguination under anesthesia and then RV free wall, left ventricle (LV) free wall, and septum tissue were harvested and weighed. RV hypertrophy was assessed by the Fulton index as the weight ratio of RV and (LV + septum). Hematocrit was obtained immediately after euthanasia.

Hemodynamic data analysis. The pressure and volume signals were recorded and at least 10 consecutive cardiac cycles free of extra systolic beats were selected and used for the analysis. Standard hemodynamic variables including heart rate (HR), RV peak systolic pressure (RVSP), total pulmonary vascular resistance (TPVR, estimated as RVSP/cardiac output) and common RV function parameters such as stroke volume (SV), stroke work (SW, estimated as the area within the PV loop), ejection fraction (EF), cardiac output (CO), chamber compliance ($\Delta V/\Delta P$), and effective arterial elastance (E_a) were exported by Notocord or calculated thereafter. RV contractile function was quantified in three ways: the slope of the ESPVR (E_{es}), preload-recruitable stroke work (PRSW), and dP/dt_{max} . RV diastolic function was further measured by dP/dt_{min} , end-diastolic volume (EDV), relaxation factor τ , and the slope of the end-diastolic pressure-volume relations (EDPVR). Finally, the RV-pulmonary vascular interaction was evaluated by ventricular-vascular coupling (VVC), a well-accepted parameter for RV function assessment in animal and clinical studies (16, 21, 42), as the ratio of E_{es} to E_a .

Preparation of skinned RV trabeculae. An additional 27 C57BL6 male mice were used for subcellular measurements of RV function. Mice were exposed to hypoxia for 0, 14, 28, or 56 days. Those exposed to hypoxia were also intraperitoneally injected with SU5416 wkly. The 0-day normoxia control mice were intraperitoneally injected with CMC vehicle for 8 wk to match the 56-day HySu animals. After euthanasia and tissue preparation, the total number of skinned RV trabeculae measurements was: $n = 6$ for 0-day HySu, $n = 10$ for 14-day HySu, $n = 12$ for 28-day HySu, and $n = 7$ for 56-day HySu.

RV trabeculae were isolated as described previously (33). All solutions were in micromoles per liter. Briefly, the hearts were removed from mice anesthetized with inhaled isoflurane and then pinned down to the dissecting dish filled with modified Ringer solution (120 NaCl, 19 NaHCO₃, 1.2 Na₂HPO₄, 1.2 MgSO₄, 5 KCl, 1 CaCl₂, 10 glucose; pH 7.4) pre-equilibrated with 95% O₂-5% CO₂. The RVs were cut open and exposed to fresh Ringer solution containing 20 mM 2,3-butanedione monoxime (BDM) for 20 min (2 \times solution change). The RV trabeculae were then dissected free, tied to sticks to hold muscle length fixed, and transferred to relaxing solution [100 KCl, 20 imidazole, 7 MgCl₂, 2 EGTA, 4 ATP, 0.25 4-(2-aminoethyl) benzenesulfonyl fluoride hydrochloride (AEBSF), 0.04 leupeptin, and 0.01 E64; pH 7.0; 4°C] containing 1% Triton X-100. After skinning overnight, the trabeculae were washed in relaxing solution (~ 1 h) and stored at -20°C in relaxing solution containing glycerol (50:50 vol/vol).

Length-tension experimental solutions, apparatus, and protocols. Solution compositions (pCa 9.0, preactivating solution, and pCa 4.5) used for mechanical measurements were calculated as previously reported (33). A range of Ca²⁺ activating solutions (pCa 6.3–5.4) were prepared by mixing solutions of pCa 9.0 and pCa 4.5.

On the day of an experiment, skinned trabeculae were washed in relaxing solution for 30 min before cutting them free from the sticks and trimming their ends. The trimmed trabeculae were then transferred to a stainless steel experimental chamber containing pCa 9.0 solution. The ends of each trabecula were attached to the arms of a motor (model 312B, Aurora Scientific) and force transducer (model 403, Aurora Scientific). The chamber assembly was then placed on the stage of an inverted microscope (Olympus) fitted with a 40 \times objective and a CCTV camera (model WV-BL600, Panasonic). Images were acquired using an AGP 4X/2X graphics card and associated

software (ATI Technologies) and were used to assess mean sarcomere length (SL) during the course of each experiment. Changes in force and motor position were sampled (16-bit resolution, DAP5216a, Microstar Laboratories) at 2.0 kHz and saved using SLControl software developed in this laboratory (<http://www.slcontrol.com>).

Passive force, Ca^{2+} activated force and apparent rate of force redevelopment (k_{tr}) were first measured at SL of 2.0 μm and then at 2.2 μm . Briefly, the skinned trabeculae were stretched to a mean SL of 2.0 μm in pCa 9.0 solution. After measuring length and width, the preparations were transferred first to preactivating solution, then to Ca^{2+} activating solution, and finally back to pCa 9.0 solution. Once in Ca^{2+} activated solution, steady-state force and the apparent rate constant of force redevelopment (k_{tr}) were measured simultaneously using the modified multistep protocol developed by Brenner and Eisenberg (33). That is, after force reached a steady level in pCa 9.0–4.5, the length was rapidly reduced by ~20%, held for 14 ms, and then restretched back to its original length. As a result of restretch, there was an initial transient increase, followed by a decrease in force (seen as a spike in the force trace) and subsequent slow recovery of force nearing the initial steady-state level. The k_{tr} is the rate constant of force redevelopment after the spike. The drop in force recorded in solution of pCa 9.0 was taken as passive force and was therefore subtracted from the drop in total force at each pCa to yield Ca^{2+} activated force (P). The protocol was repeated to establish active force-pCa and k_{tr} -pCa/relative active force at SL of 2.2 μm .

RV trabeculae data analysis. Cross-sectional areas of skinned trabeculae were calculated assuming that the trabeculae are cylindrical and using the widths measured from video images. Each Ca^{2+} activated force (P) at pCa between 6.4 and 5.4 was expressed as a fraction of the maximum Ca^{2+} activated force (P_o) developed by the same preparations at pCa 4.5, i.e., P/P_o . To determine the Ca^{2+} sensitivity of isometric force (pCa₅₀), force-pCa data were fitted with the Hill equation: $P/P_o = [\text{Ca}^{2+}]^n / (k^n + [\text{Ca}^{2+}]^n)$, where n is the slope (n_H ; Hill coefficient) and k is the Ca^{2+} concentration for half-maximal activation (pCa₅₀). k_{tr} was determined by linear transformation of the half-time of force recovery [$k_{tr} = -\ln 0.5 \times (t_{1/2})^{-1}$] (33).

RV histology and immunohistochemistry. In additional groups of mice exposed to HySu for 0, 14, and 56 days ($N = 4$ per group), RV tissues were harvested, fixed in 10% formalin, paraffin embedded, and longitudinally sectioned for histology analysis. H&E stain was performed to examine the cardiomyocyte morphology, and immunohistochemistry was performed to examine the RV capillary rarefaction and RV calcium handling capability. Briefly, sections were deparaffinized, rehydrated, heated in pH 6.0 citrate solution (10 mM citric acid, 0.05% Tween 20) to induce epitope retrieval, and incubated with 0.3% H_2O_2 to inactivate endogenous peroxidase. Sections were then blocked with 10% goat serum (Sigma, St. Louis, MO), stained with rabbit polyclonal anti-human von Willebrand factor (vWF) (1:100, ab7356, previously Chemicon International and now MilliporeSigma, Temecula, CA), and visualized with Signal Stain Boost IHC Detection Reagent (Cell Signaling Technology, Beverly, MA) and DAB substrate kit (8059, Cell Signaling, Danvers, MA). Finally, slides were counterstained with hematoxylin.

Images were captured using an inverted microscope (TE-2000–5, Nikon, Melville, NY) and analyzed using MetaVue (Optical Analysis Systems, Nashua, NH). The cardiomyocyte morphology was measured by 1) the cell area under the cross-section orientation and 2) the cardiomyocyte width (or diameter) under the longitudinal orientation at positions presenting substantial length of uniform width (44). For each animal, 5–10 regions were selected and averaged to derive the myocyte cross-sectional area (CSA) or width. For immunostaining images, the positive staining area (i.e., the brown color) was identified by color thresholding in a representative field. This area was then divided by the entire vessel area to calculate the area percentage of vWF expression. All histology analyses were done by an individual

observer blinded to the condition/group of the histology slides during the quantification.

Statistical analysis. Statistical analysis of in vivo hemodynamics was performed using a one-way ANOVA with Tukey HSD test for exposure groups or generalized least squares with multiple comparisons for exposure. Data analysis was conducted using the R software version 2.5.1 (R Foundation for Statistical Computing, Vienna, Austria). For the RV trabeculae analysis, either paired or unpaired t -tests were used. All P values were two-sided, and $P < 0.05$ was taken as statistically significant. All values are presented as means \pm SE.

RESULTS

Progression of PAH. RVSP increased progressively as HySu exposure time increased up to 28 days (control group = 0-day HySu) and then plateaued ($P < 0.05$, Fig. 1A). The increase in RVSP tracked the increases in total PVR (see Table 2, $P < 0.05$) and E_a ($P < 0.05$, Fig. 1B).

RV hypertrophy was significant in early PAH and did not further advance in later PAH (see RV mass and Fulton index in Table 1, $P < 0.05$). Mice in all HySu exposure groups had increased hematocrit (Table 1, $P < 0.05$) as expected. We did not observe significant changes in mean aortic pressure (MAP) in early PAH groups; there was a small but significant increase in MAP in the 56-day HySu group (Table 1). No LV hypertrophy was present in any PAH group compared with control.

RV function at organ level. We quantified organ-level RV contractile function by PRSW (Table 2), dP/dt_{\max} , and E_{es} (ESPVR) (Fig. 1, C and D). As measured by the first two parameters, RV contractility increased at an early stage (14-day HySu) and then plateaued. In contrast, the preload independent contractility (E_{es}) increased initially (at 14- and 28-day HySu) and then returned to control levels (at 56-day HySu) (Fig. 1D).

We also measured parameters that are typically used to evaluate overall heart function in vivo: EF and SV. With the progression of PAH, EF gradually decreased and the reduction reached significance at the 56-day point (Fig. 1E, $P < 0.05$). We observed a trend of reduction in SV but no changes were statistically significant (Table 1). There were no significant changes in either heart rate (Table 1) or CO (Table 2).

The ventricular-vascular coupling (VVC), computed as E_{es}/E_a , is a useful functional index to capture the ability of the RV to supply blood flow to the pulmonary circulation against a given arterial afterload (42). This parameter assesses the organ-organ interaction of the entire RV-pulmonary vasculature system. We found that VVC was maintained in early, mild PAH (14-day HySu) and fell with later, more severe PAH (56-day HySu, $P < 0.05$, Fig. 1F) due to the persistent increase in arterial afterload (E_a) with control-level RV contractility (E_{es}).

To assess RV diastolic function, we measured RV chamber wall compliance, end-diastolic volume (EDV), dP/dt_{\min} , relaxation factor (τ), and the end-diastolic pressure-volume relationship (EDPVR) (see Table 2). We observed a significant decrease in RV chamber compliance since early PAH ($P < 0.05$), suggesting RV wall stiffening occurred in all stages of PAH. RV EDV increased significantly in the 56-day HySu group ($P < 0.05$), indicating the RV dilation at late PAH. dP/dt_{\min} was markedly reduced at early PAH and continued decreasing with increased HySu exposure duration ($P < 0.05$). There was a significant decrease in τ , a preload-independent measure of isovolumic relaxation, with early PAH, but τ returned toward

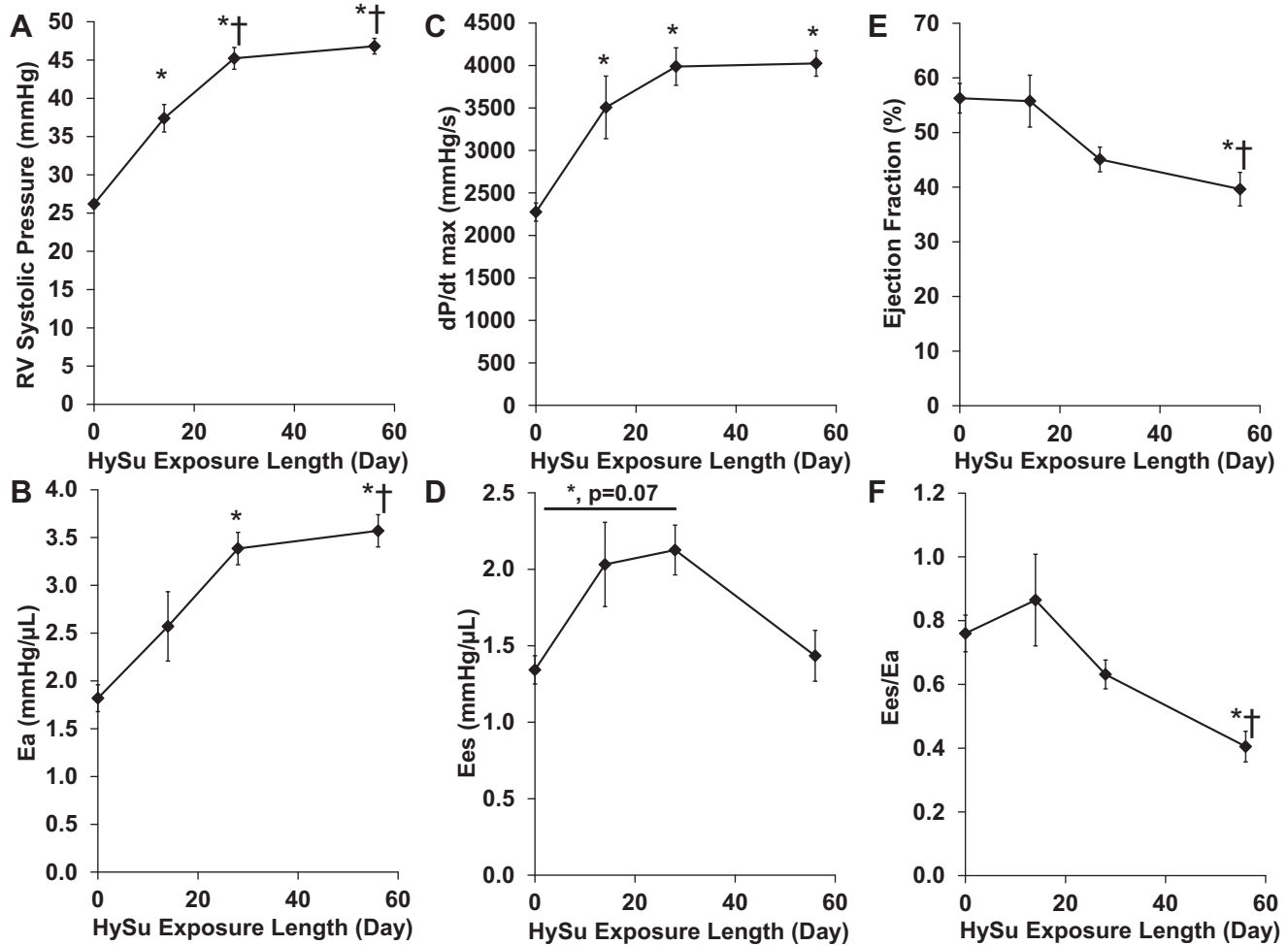


Fig. 1. Changes in RV systolic pressure (A), total arterial afterload E_a (B), dP/dt_{max} (C), E_{es} (D), ejection fraction (E), and ventricular-vascular coupling (E_{es}/E_a) (F) after 14-, 28- and 56-day HySu exposure. * $P < 0.05$ vs. normoxia. † $P < 0.05$ vs. 14-day HySu. $N = 8-9$ per group.

control levels in the 28-HySu and 56-day HySu groups ($P < 0.05$). Finally, we did not observe significant changes in the EDPVR in any PAH group.

RV function at subcellular level. The passive force generated by RV trabeculae at different sarcomere lengths (SL) was measured, and the SL-dependent changes in passive force were identical in all groups. At SL 2.0 μ m, passive force measured in all PAH trabeculae was similar to the control, and at longer SLs, the passive force was elevated in all PAH trabeculae and

there was no difference in PAH groups (Fig. 2A). Detailed results are presented in Table 3.

Next, we examined the maximal Ca^{2+} -activated force at different SL. All PAH groups showed significantly elevated activated force at every SL except for the 56-day HySu group at SL 2.2 μ m (Table 3). When trabeculae were stretched from SL 2.0 to 2.2 μ m, there was a significant increase in maximum Ca^{2+} -activated force in both control and PAH trabeculae (Table 3). Thus SL-dependent increases in maximum Ca^{2+} -activated force were evident and similar in all groups of trabeculae.

We also examined Ca^{2+} sensitivity of force (pCa_{50}) in the RV trabeculae. The time-dependent changes in pCa_{50} were different from those observed in passive or maximal Ca^{2+} -activated forces. Interestingly, pCa_{50} was significantly higher in 14-day HySu trabeculae compared with control trabeculae, and this increase was absent in 28- and 56-day HySu trabeculae (Fig. 2B). When stretched from SL 2.0 to 2.2 μ m, the pCa_{50} values increased in all four groups of trabeculae. Thus SL-dependent increases in Ca^{2+} sensitivity of force were evident and similar in all groups of trabeculae.

Finally, at both SLs, the Hill coefficient (n_H) and the apparent rate of maximum force redevelopment (k_{tr}) were similar in

Table 1. Changes in whole body parameters after 14-, 28- and 56-day HySu exposure

	Normoxia	14-day HySu	28-day HySu	56-day HySu
RV mass, mg	20 \pm 1	31 \pm 2*	34 \pm 2*	32 \pm 2*
LV + septum mass, mg	78.3 \pm 2.2	77.8 \pm 4.3	78.9 \pm 4.5	74.0 \pm 4.6
BW, g	25.3 \pm 0.6	23.2 \pm 0.4	24.1 \pm 0.6	24.4 \pm 0.7
Fulton index, mg/mg	0.26 \pm 0.01	0.40 \pm 0.02*	0.44 \pm 0.03*	0.43 \pm 0.01*
Hct, %	46 \pm 1.1	75 \pm 2.2*	61 \pm 0.4*	69 \pm 1.0*
HR, beats/min	552 \pm 16	597 \pm 17	597 \pm 17	602 \pm 14
MAP, mmHg	53 \pm 5	55 \pm 3	55 \pm 1	72 \pm 3*†#

Results are presented as means \pm SE; $n = 8-9$ per group. RV, right ventricle; LV, left ventricle; S, septum; BW, body weight; Hct, hematocrit. * $P < 0.05$ vs. Normoxia. † $P < 0.05$ vs. 14-day HySu. # $P < 0.05$ vs. 28-day HySu.

Table 2. Changes in pulmonary and RV hemodynamics after 14-, 28- and 56-day HySu exposure

	Normoxia	14-day HySu	28-day HySu	56-day HySu
Total PVR, mmHg·ml ⁻¹ ·min	3.3 ± 0.3	4.5 ± 0.5	5.6 ± 0.3*	5.8 ± 0.3*
PRSW, mmHg	19 ± 1	28 ± 3	26 ± 1	27 ± 2
RV EDV, μl	24 ± 1	26 ± 3	30 ± 1	35 ± 2*
RVEDP, mmHg	0.8 ± 0.1	1.2 ± 0.1	1.4 ± 0.2*	1.1 ± 0.1
RV compliance, μl/mmHg	0.53 ± 0.03	0.36 ± 0.04*	0.30 ± 0.01*	0.29 ± 0.01*
τ, ms	5.7 ± 0.5	3.1 ± 0.6*	5.0 ± 0.3	5.3 ± 0.5†
dP/dt _{min} , mmHg/s	1,657 ± 213	2,630 ± 195*	3,525 ± 161*†	3,480 ± 138*†
RV ESV, μl	9.8 ± 0.6	12.4 ± 2.6	16.5 ± 1.3	21.2 ± 2.3
SV, μl	14.7 ± 1.0	14.9 ± 1.4	13.4 ± 0.7	13.4 ± 0.7
CO, ml/min	8.1 ± 0.6	8.9 ± 0.9	8.0 ± 0.5	8.0 ± 0.4
EDPVR, mmHg/μl	0.08 ± 0.01	0.08 ± 0.01	0.09 ± 0.01	0.07 ± 0.01

Results are presented as means ± SE; *n* = 8–9 per group. PVR, pulmonary vascular resistance; PRSW, preload recruitable stroke work; RV EDV, RV end-diastolic volume; RVEDP, RV end-diastolic pressure (RVEDP, mmHg), τ, relaxation factor; RV ESV, RV end-systolic volume; SV, stroke volume; CO, cardiac output; EDPVR, end-diastolic pressure-volume relationship. **P* < 0.05 vs. Normoxia. †*P* < 0.05 vs. 14-day HySu.

PAH and control trabeculae, and all PAH trabeculae redeveloped maximum force at similar rates as control (Table 3). When stretched from SL 2.0 to 2.2 μm, there were a decrease in n_H values and a small but insignificant decrease in k_{tr} in all four groups of trabeculae.

Morphological and biological changes in RV cardiomyocyte. Because we found some differences in RV function between early- and late-PAH groups, we further investigated the structural changes in these RVs as well as the control RVs (i.e., normoxia, 14-day HySu and 56-day HySu groups). We examined the cardiomyocyte morphology with 2 different orientations. In the cross-sectional orientation, the RV myocyte CSA was increased similarly at both early and late PAH (Fig. 3, A–D; *P* < 0.05). In contrast, with the longitudinal orientation, the RV myocyte width was increased only in late PAH (Fig. 3, E–H; *P* < 0.05). In addition, qualitatively, the cell alignment was well-organized in control and early PAH and became disorganized (loss of parallel striation and increased waviness) in late PAH (Fig. 3, E–G). These morphological changes indicated that the hypertrophy index of myocyte width, not myocyte CSA, is distinct in RV of late PAH from RV of early PAH.

We further measured the expression of vWF in blood vessels in these RVs. As vWF is routinely expressed by healthy

endothelial cells, the amount of vWF expression is a good indicator of coronary artery perfusion in RVs (54, 56). As shown in Fig. 3, I and J, both early and late PAH had similarly decreased vWF expression in RVs (*P* < 0.05). Thus coronary perfusion is likely impaired early in PAH development.

DISCUSSION

In the present study, we examined the temporal changes in RV structure and function at the organ level and subcellular level using a mouse model of PAH that displays many of the hallmarks of the human disease (4). The main finding is that the initiation of RV dysfunction due to chronic pressure overload was accompanied by no impairment of the Frank-Starling mechanism in the myofilaments. Specifically, we found that with pressure overload: 1) RV EF decreases and RV contractility becomes uncoupled from the afterload (i.e., VVC decreases) in late PAH, indicating RV dysfunction; 2) in both early and late PAH, RV trabeculae passive force increases and RV wall compliance decreases, suggesting that ventricular stiffening is universally present during the progression of RV dysfunction; 3) in all PAH groups, the Frank-Starling mechanism is preserved in cardiac trabeculae; 4) myocyte CSA was increased and RV vWF expression was decreased since early

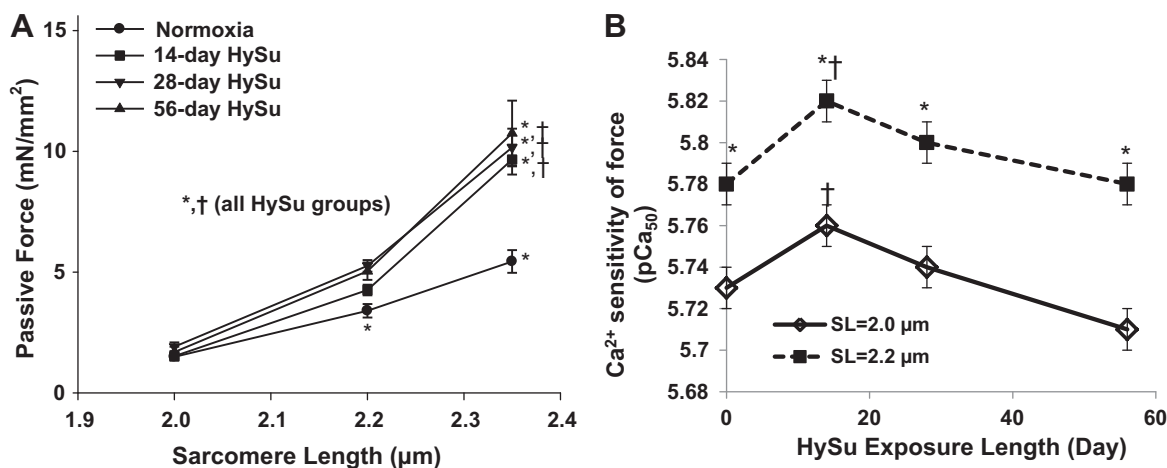


Fig. 2. Changes in SL-dependent changes in passive force (A) and Ca²⁺ sensitivity of force (pCa₅₀) (B) in skinned RV trabeculae. The measurements were done in skinned normoxia (*n* = 6), 14-day HySu (*n* = 10), 28-day HySu (*n* = 12), and 56-day HySu (*n* = 7) RV trabeculae. **P* < 0.05 vs. SL = 2.0 μm in the same trabeculae. †*P* < 0.05 vs. normoxia at the same SL.

Table 3. Summary of SL-dependent changes in mechanical properties of skinned RV trabeculae

SL, μm	Passive Force, mN/mm^2	Maximum Ca^{2+} Activated Force, mN/mm^2	Hill Coefficient, n_H	Ca^{2+} Sensitivity of Force, pCa_{50}	Maximum Rate of Force Redevelopment, (k_{tr}), s^{-1}
<i>Normoxia (6/6)</i>					
2.0	1.49 ± 0.15	25.52 ± 1.28	2.42 ± 0.04	5.73 ± 0.01	32.82 ± 2.11
2.2	$3.40 \pm 0.28^*$	$35.23 \pm 2.78^*$	2.40 ± 0.04	$5.78 \pm 0.01^*$	31.46 ± 2.11
<i>14-day HySu (10/7)</i>					
2.0	1.52 ± 0.11	$34.32 \pm 1.54^\#$	2.50 ± 0.08	$5.76 \pm 0.01^\#$	31.52 ± 0.74
2.2	$4.26 \pm 0.22^{*\#}$	$45.88 \pm 2.16^{*\#}$	$2.42 \pm 0.06^*$	$5.82 \pm 0.01^{*\#}$	29.83 ± 0.85
<i>28-day HySu (12/7)</i>					
2.0	1.91 ± 0.18	$34.91 \pm 2.49^\#$	2.35 ± 0.03	5.74 ± 0.01	33.41 ± 1.50
2.2	$5.26 \pm 0.24^{*\#}$	$46.75 \pm 2.98^{*\#}$	$2.26 \pm 0.02^*$	$5.80 \pm 0.01^*$	32.70 ± 1.31
<i>56-day HySu (7/7)</i>					
2.0	1.69 ± 0.22	$33.16 \pm 2.75^\#$	2.41 ± 0.08	5.71 ± 0.01	31.83 ± 1.57
2.2	$5.04 \pm 0.36^{*\#}$	$44.12 \pm 5.07^*$	2.34 ± 0.05	$5.78 \pm 0.01^*$	31.21 ± 1.77

All values are expressed as means \pm SE, with the no. of skinned RV trabeculae/mice hearts given in parentheses. *Significantly different from values recorded at SL = 2.0 μm . #Significantly different from values recorded at the same SL in normoxia trabeculae.

PAH, suggesting cell enlargement and impaired myocardial perfusion contribute to the organ hypertrophy and dysfunction; and 5) myocyte width was increased only in late PAH, suggesting increased myocyte width rather than increased CSA is a morphological signature of RV dysfunction.

The cause of death in severe PAH is typically RV failure. However, RV failure is a complex process and our current understanding of RVF is at a preliminary stage, largely shaped by the literature on left ventricle (LV) failure (5, 30, 37). It has become increasingly clear that, due to the differences in embryologic origin, anatomy, and function, the pathologies of the

two chambers are quite distinct (9). Indeed, a unique feature of RVF secondary to PAH is its reversibility after lung transplant (13). This suggests that the RV maladaptation is recoverable and probably due to different mechanisms at the organ level and the cellular level.

The development of pressure overload-induced RV dysfunction, which ultimately leads to RV failure, is poorly understood. A recent consensus concerning right heart failure defines it as "a clinical syndrome due to an alteration of structure and/or function of right heart circulatory system that leads to sub-optimal delivery of blood flow (high or low) to the pul-

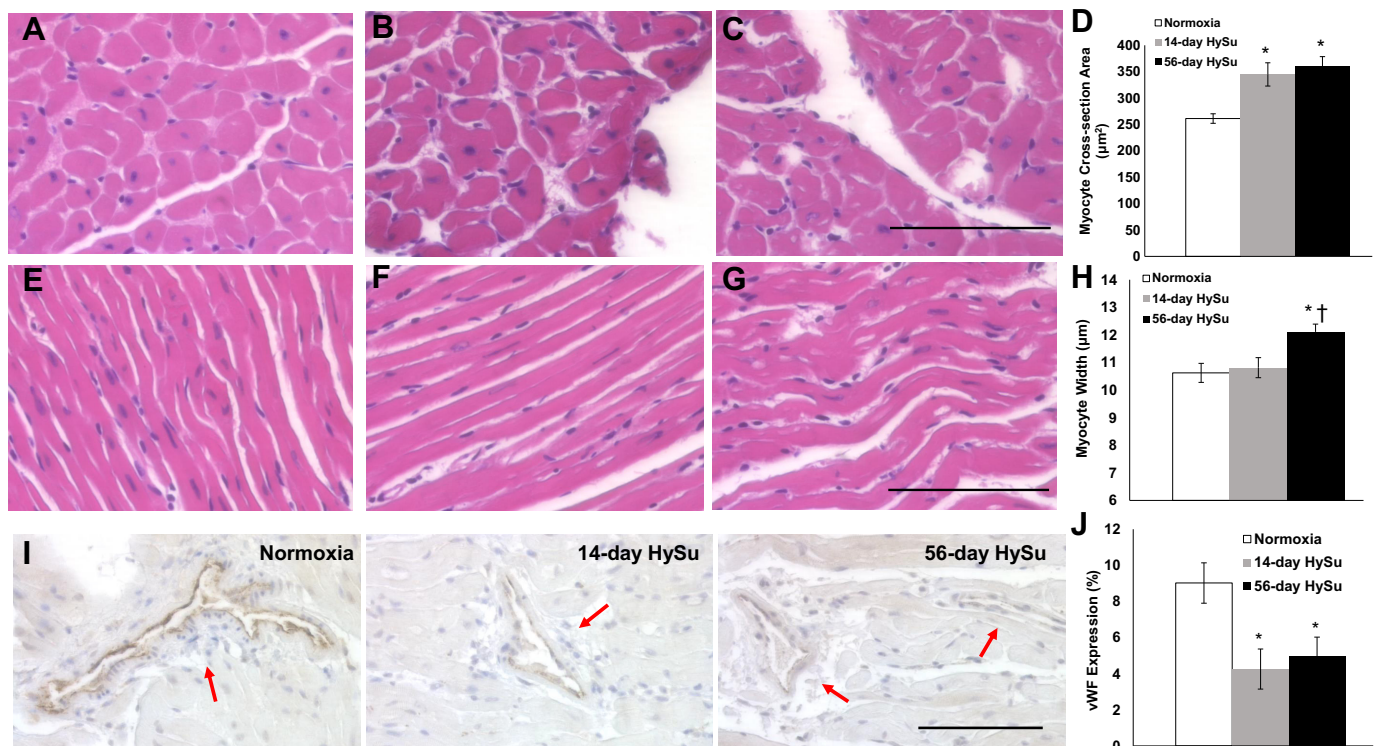


Fig. 3. Morphological and molecular changes in RVs. A–C: representative histology images of cross-section orientation of myocytes from normoxia, 14-day, and 56-day HySu groups. D: myocyte cross-sectional area changes in these RVs. E–G: representative histology images of longitudinal orientation of myocytes from Normoxia, 14-day, and 56-day HySu groups. H: myocyte width changes in these RVs. I: representative histological images of RVs stained for vWF expression (brown color) in Normoxia, 14-day, and 56-day HySu groups. Arrows indicates blood vessels found in RV tissues. J: vWF expression level changes in these RVs. * $P < 0.05$ vs. normoxia. † $P < 0.05$ vs. 14-day HySu. $N = 4$ per group. Scale bar, 50 μm .

monary circulation and/or elevated venous pressures—at rest or with exercise” (30). Due to a lack of clinical definition of RV failure with cut-off values for functional parameters (e.g., in RV EF or CO), prior studies include heterogeneous phenotypes of RV structure and function at different time points, severity, and species (3, 4, 8, 36, 39, 41, 49). Moreover, most studies examine RV function at either the organ level or cellular level but not both. To date, the present study is the first to investigate the development of RV dysfunction, in a time-dependent manner, at both the organ level and myocyte level.

Transition from RV function to dysfunction at whole organ level. We observed continuous PAH progression as evidenced by the monotonically increasing total PVR, arterial afterload (E_a), RVSP, PRSW, dP/dt_{max} , and dP/dt_{min} ; and, with the persistent pressure overload, the RV chamber dilated and EF decreased significantly, which are often observed in failing RV (48).

The progression of RV dysfunction was more pronounced in the changes in ventricular-vascular coupling (VVC; E_{es}/E_a). In early PAH (up to 14-day HySu), preload-independent RV contractility measured by ESPVR (E_{es}) increased to match the increased arterial afterload, and as a result, VVC was maintained (Fig. 1). This increased contractile function was accompanied by an increase in RV mass (see Fulton index in Table 1) and no increase in RV chamber size (see RV EDV in Table 2). Thus overall, organ function was preserved. From 28-day HySu to 56-day HySu, which is late PAH, ESPVR was not able to match the continuously increased afterload, and VVC started to drop with the reduction being significant in the 56-day HySu group (Fig. 1). In this most severe PAH group, RV mass did not further increase compared with early PAH, EF was significantly decreased, and RV chamber volume was significantly increased. Thus the organ function was impaired.

Absence of impairment in Frank-Starling relations at sub-cellular level despite RV dysfunction at whole organ level. Whereas we observed time-dependent changes in RV function at the whole organ level, the investigation of RV trabeculae revealed different time-dependent cellular changes. More importantly, at all time points, the SL-dependent changes in RV trabeculae mechanical properties in PAH were similar to healthy controls, indicating that the Frank-Starling mechanism was preserved in PAH RVs.

Ca^{2+} sensitivity of force (pCa_{50}) was higher than in control trabeculae only in the 14-day HySu trabeculae (Fig. 2B, $P < 0.05$) and then started to decrease at later time points (Fig. 2B). Changes in myofilament calcium sensitivity is a primary cause of reduced contractile performance of the heart although disparate results have been found between rodent studies and human studies, i.e., high Ca^{2+} sensitivity is found in human failing LVs but low Ca^{2+} sensitivity is found in some animal failing LVs (28). Thus in LV failure, both increased and decreased Ca^{2+} sensitivity have been reported (27, 28, 46). Inconsistent reports of changes in Ca^{2+} sensitivity are similarly found in RV failure research. A decrease in pCa_{50} has been found in hypoxic neonatal calves RVs (49), but no change in Ca^{2+} sensitivity is reported in PAH patient RVs (36), monocrotaline-induced failing rat RVs (tested near physiological frequency) (23) or in pulmonary arterial banding (PAB) rat RVs (8). Thus changes in pCa_{50} are variable and may be dependent on the stage or severity of the heart failure or experimental procedures adopted (including the choice of con-

trols) or animal model used. More interestingly, our results concerning the time-dependent changes in pCa_{50} agree with the hypothesis of de Tombe (28) that heart failure is associated with early increase in myofilament Ca^{2+} sensitivity that reverts to decreased Ca^{2+} sensitivity at end-stage heart failure.

SL-dependent increases in passive force, maximum Ca^{2+} -activated force, and Ca^{2+} sensitivity of force were observed in all RV trabeculae, confirming prior reports in healthy rat trabeculae (19, 33), healthy mouse trabeculae and myocytes (6, 20, 24), healthy bovine and porcine ventricular strips (6, 10, 43), healthy human ventricular myocytes (6, 45), as well as ventricles with pulmonary pressure overload from a variety of species [in rat (8), calf (49) and human (36)]. Previous in vitro studies on failing human LVs have yielded conflicting results: whereas some reported the Frank-Starling mechanism to be abolished (40), others showed that the length-tension relationship is preserved (52). In contrast, the findings on RVs with pressure overload are very clear as all studies report a preserved Frank-Starling mechanism (8, 36, 49), including our own data.

At SL $>2.0 \mu m$, the passive force measured in all PAH trabeculae was significantly higher than that of the normoxia trabeculae (Fig. 2A, $P < 0.05$), and there were no further time- or severity-dependent changes in passive force. This initial increase in passive force was also reported in PAH patients with diastolic dysfunction defined as increased EDPVR (36). The increased length-dependent passive force, as a significant cellular change in the PAH trabeculae, could affect the organ-level pressure-volume relationships and right heart hemodynamics. Here we did not observe significant changes in EDPVR or τ ; however, there was a significant reduction in RV chamber compliance, RV dilation, and increase in dP/dt_{min} (Table 2, $P < 0.05$). These changes suggest a stiffened ventricular wall and enlarged chamber with increased rate of isovolumic relaxation (dP/dt_{min}).

Since titin and collagen predominantly contribute to passive force in myocardium (15, 35, 53), the increase in passive force in PAH trabeculae may be due to changes in either titin isoform type/phosphorylation state or collagen isoform type/content or both. Here we did not examine the titin in mouse RVs, but we have previously reported an increased collagen accumulation in the RVs of the same mouse PAH model (51), which suggests that the elevated passive force may be due to changes in collagen expression and subsequent fibrosis.

Cellular and molecular changes associated with RV dysfunction. In addition to the functional changes, we examined the structural changes in these RVs via histology and immunohistochemistry. Cardiomyocyte morphology is an important indicator of cardiac hypertrophy and the commonly examined parameters include myocyte CSA, length, width, and volume (36, 38). Here we observed a similar degree of CSA increase (~40%) in 14-day and 56-day HySu RVs. Since the same changes were observed in RV mass increase (Table 1), our results demonstrate that CSA enlargement contributes to the organ-level hypertrophy. Moreover, neither the RV mass nor the myocyte CSA further increased in late PAH when RV dysfunction occurred, which is consistent with prior findings that myocyte CSA does not increase with transition to failure in LVs in either hypertensive (11, 32) or myocardial infarction subjects (12, 55). The exact subcellular changes during myocyte CSA enlargement are unclear, and it is unknown how

these changes contribute to the development of RV dysfunction.

In contrast, the myocyte width measurement showed a significant increase in dysfunctional RVs from late PAH, and there was no increase in RVs from early PAH. Therefore, myocyte width may be a useful morphological marker for RV dysfunction. Although myocyte lengthening is associated with heart failure in LVs (11), it is challenging to measure in histological thin sections of tissue. This first report of the RV myocyte morphology change in dysfunctional RVs suggests myocyte width rather than CSA could be used as a simply measured cellular signature of RV dysfunction.

At the molecular level, the vWF expression, which measures endothelial cell function in coronary vessels, was reduced in RVs of both early and late PAH. These data suggest that impaired myocardial perfusion may be an additional key factor underlying the progression of RV dysfunction. Abnormal coronary circulation such as decreased vascular density (34) or RV ischemia (14) has been reported in failing human RVs. Moreover, an miRNA-126 treatment designed to improve RV vascular density has been shown to reverse RV failure in a rat model of PAH (14). This evidence not only suggests an important role of myocardial perfusion in RV dysfunction progression but also indicates that myocyte impairment may be limited (e.g., with preserved Frank-Starling mechanism) so that the RV dysfunction/failure is reversible (13).

RV dysfunction and failure: understanding of mechanisms. Presently there is no clear clinical definition of RV failure, probably due to the lack of detailed cellular and molecular mechanisms to explain RVF (47, 48). At the physiological level, RV failure has been identified by reduction in CO, SV, and/or EF, RV wall dilation, or decrease in contractility or VVC. But not all of these parameters are able to consistently predict RV failure: in some cases RV contractility increases as an adaptive response but SV or CO decreases, fulfilling a definition of failure (25); in other cases, the failing RV has reduced EF and diastolic dysfunction yet preserved CO (36). A recent study on sex differences in PAH patients suggests EF may be a more sensitive parameter for disease progression than CO (18). Therefore, it is necessary to understand the progression of RV dysfunction (and ultimately RV failure) to better care for patients.

In our late-PAH group (56-day HySu), we observed significant decreases in VVC and EF accompanied by RV chamber dilatation (EDV increase), and these data strongly indicate RV dysfunction. However, none of the PAH groups showed decreased SV or CO, which suggests a lack of established RV failure. Therefore, our experimental study captured the initiation of RV dysfunction, not an end-stage RV failure, due to chronic pressure overload. More importantly, the simultaneous examination of functional changes at whole organ and subcellular levels reveals time-dependent functional changes at the whole organ level accompanied by preserved Frank-Starling mechanism at the myocyte level.

ACKNOWLEDGMENTS

We thank Dr. Guoqing Song for the surgical assistance in pressure-volume loop measurements and Dr. Jens C. Eickhoff for the assistance in statistical analysis.

GRANTS

This study is funded by National Heart, Lung, and Blood Institute Grants R01-HL-086939 and R01-HL-115061.

DISCLOSURES

No conflicts of interest, financial or otherwise, are declared by the authors.

AUTHOR CONTRIBUTIONS

Z.W. and N.C.C. conceived and designed research; Z.W., J.R.P., D.A.S., and T.A.H. performed experiments; Z.W., J.R.P., and D.A.S. analyzed data; Z.W., J.R.P., T.A.H., R.L.M., and N.C.C. interpreted results of experiments; Z.W. prepared figures; Z.W. and J.R.P. drafted manuscript; Z.W., J.R.P., D.A.S., T.A.H., R.L.M., and N.C.C. edited and revised manuscript; Z.W., J.R.P., D.A.S., T.A.H., R.L.M., and N.C.C. approved final version of manuscript.

REFERENCES

- Bartelds B, Borgdorff MA, Smit-van Oosten A, Takens J, Boersma B, Nederhoff MG, Elzenga NJ, van Gilst WH, De Windt LJ, Berger RM. Differential responses of the right ventricle to abnormal loading conditions in mice: pressure vs. volume load. *Eur J Heart Fail* 13: 1275–1282, 2011. doi:10.1093/eurjhf/hfr134.
- Boehm M, Lawrie A, Wilhelm J, Ghofrani HA, Grimminger F, Weissmann N, Seeger W, Schermuly RT, Kojonazarov B. Maintained right ventricular pressure overload induces ventricular-arterial decoupling in mice. *Exp Physiol* 102: 180–189, 2017. doi:10.1113/EP085963.
- Borgdorff MAJ, Bartelds B, Dickinson MG, Steendijk P, de Vroomen M, Berger RMF. Distinct loading conditions reveal various patterns of right ventricular adaptation. *Am J Physiol Heart Circ Physiol* 305: H354–H364, 2013. doi:10.1152/ajpheart.00180.2013.
- Ciucan L, Bonneau O, Hussey M, Duggan N, Holmes AM, Good R, Stringer R, Jones P, Morrell NW, Jarai G, Walker C, Westwick J, Thomas M. A novel murine model of severe pulmonary arterial hypertension. *Am J Respir Crit Care Med* 184: 1171–1182, 2011. doi:10.1164/rccm.201103-0412OC.
- Drake JI, Bogaard HJ, Mizuno S, Clifton B, Xie B, Gao Y, Dumur CI, Fawcett P, Voelkel NF, Natarajan R. Molecular signature of a right heart failure program in chronic severe pulmonary hypertension. *Am J Respir Cell Mol Biol* 45: 1239–1247, 2011. doi:10.1165/rcmb.2010-0412OC.
- Edes IF, Czuriga D, Csányi G, Chlopicki S, Recchia FA, Borbély A, Galajda Z, Edes I, van der Velden J, Stienen GJ, Papp Z. Rate of tension redevelopment is not modulated by sarcomere length in permeabilized human, murine, and porcine cardiomyocytes. *Am J Physiol Regul Integr Comp Physiol* 293: R20–R29, 2007. doi:10.1152/ajpregu.00537.2006.
- Faber MJ, Dalinghaus M, Lankhuizen IM, Steendijk P, Hop WC, Schoemaker RG, Duncker DJ, Lamers JM, Helbing WA. Right and left ventricular function after chronic pulmonary artery banding in rats assessed with biventricular pressure-volume loops. *Am J Physiol Heart Circ Physiol* 291: H1580–H1586, 2006. doi:10.1152/ajpheart.00286.2006.
- Fan D, Wannenburg T, de Tombe PP. Decreased myocyte tension development and calcium responsiveness in rat right ventricular pressure overload. *Circulation* 95: 2312–2317, 1997. doi:10.1161/01.CIR.95.9.2312.
- Friedberg MK, Redington AN. Right versus left ventricular failure: differences, similarities, and interactions. *Circulation* 129: 1033–1044, 2014. doi:10.1161/CIRCULATIONAHA.113.001375.
- Fukuda N, Wu Y, Farman G, Irving TC, Granzier H. Titin isoform variance and length dependence of activation in skinned bovine cardiac muscle. *J Physiol* 553: 147–154, 2003. doi:10.1113/jphysiol.2003.049759.
- Gerdes AM. Cardiac myocyte remodeling in hypertrophy and progression to failure. *J Card Fail* 8, Suppl: S264–S268, 2002. doi:10.1054/jcaf.2002.129280.
- Gerdes AM, Kellerman SE, Moore JA, Muffly KE, Clark LC, Reaves PY, Malec KB, McKeown PP, Schocken DD. Structural remodeling of cardiac myocytes in patients with ischemic cardiomyopathy. *Circulation* 86: 426–430, 1992. doi:10.1161/01.CIR.86.2.426.
- Globits S, Burghuber OC, Koller J, Schenk P, Frank H, Grimm M, End A, Glogar D, Imhof H, Klepetko W. Effect of lung transplantation on right and left ventricular volumes and function measured by magnetic

- resonance imaging. *Am J Respir Crit Care Med* 149: 1000–1004, 1994. doi:10.1164/ajrccm.149.4.8143034.
14. Gómez A, Bialostozky D, Zajarias A, Santos E, Palomar A, Martínez ML, Sandoval J. Right ventricular ischemia in patients with primary pulmonary hypertension. *J Am Coll Cardiol* 38: 1137–1142, 2001. doi:10.1016/S0735-1097(01)01496-6.
 15. Granzier HL, Irving TC. Passive tension in cardiac muscle: contribution of collagen, titin, microtubules, and intermediate filaments. *Biophys J* 68: 1027–1044, 1995. doi:10.1016/S0006-3495(95)80278-X.
 16. Guihaire J, Haddad F, Boulate D, Decante B, Denault AY, Wu J, Hervé P, Humbert M, Darteville P, Verhoye JP, Mercier O, Fadel E. Non-invasive indices of right ventricular function are markers of ventricular-arterial coupling rather than ventricular contractility: insights from a porcine model of chronic pressure overload. *Eur Heart J Cardiovasc Imaging* 14: 1140–1149, 2013. doi:10.1093/ehjci/jet092.
 17. Humbert M, Sitbon O, Chaouat A, Bertocchi M, Habib G, Gressin V, Yaïci A, Weitzenblum E, Cordier JF, Chabot F, Dromer C, Pison C, Reynaud-Gaubert M, Haloun A, Laurent M, Hachulla E, Cottin V, Degano B, Jais X, Montani D, Souza R, Simonneau G. Survival in patients with idiopathic, familial, and anorexigen-associated pulmonary arterial hypertension in the modern management era. *Circulation* 122: 156–163, 2010. doi:10.1161/CIRCULATIONAHA.109.911818.
 18. Jacobs W, van de Veerdonk MC, Trip P, de Man F, Heymans MW, Marcus JT, Kawut SM, Bogaard HJ, Boonstra A, Vonk Noordegraaf A. The right ventricle explains sex differences in survival in idiopathic pulmonary arterial hypertension. *Chest* 145: 1230–1236, 2014. doi:10.1378/chest.13-1291.
 19. Konhilas JP, Irving TC, de Tombe PP. Myofilament calcium sensitivity in skinned rat cardiac trabeculae: role of interfilament spacing. *Circ Res* 90: 59–65, 2002. doi:10.1161/hh0102.102269.
 20. Konhilas JP, Irving TC, Wolska BM, Jweid EE, Martin AF, Solaro RJ, de Tombe PP. Troponin I in the murine myocardium: influence on length-dependent activation and interfilament spacing. *J Physiol* 547: 951–961, 2003. doi:10.1113/jphysiol.2002.038117.
 21. Kubba S, Davila CD, Forfia PR. Methods for evaluating right ventricular function and ventricular-arterial coupling. *Prog Cardiovasc Dis* 59: 42–51, 2016. doi:10.1016/j.pcad.2016.06.001.
 22. Kuehne T, Yilmaz S, Steendijk P, Moore P, Groenink M, Saeed M, Weber O, Higgins CB, Ewert P, Fleck E, Nagel E, Schulze-Neick I, Lange P. Magnetic resonance imaging analysis of right ventricular pressure-volume loops: in vivo validation and clinical application in patients with pulmonary hypertension. *Circulation* 110: 2010–2016, 2004. doi:10.1161/01.CIR.0000143138.02493.DD.
 23. Lamberts RR, Hamdani N, Soekhoe TW, Boontje NM, Zaremba R, Walker LA, de Tombe PP, van der Velden J, Stienen GJ. Frequency-dependent myofilament Ca²⁺ desensitization in failing rat myocardium. *J Physiol* 582: 695–709, 2007. doi:10.1113/jphysiol.2007.134486.
 24. Lee E-J, Peng J, Radke M, Gotthardt M, Granzier HL. Calcium sensitivity and the Frank-Starling mechanism of the heart are increased in titin N2B region-deficient mice. *J Mol Cell Cardiol* 49: 449–458, 2010. doi:10.1016/j.yjmcc.2010.05.006.
 25. Leeuwenburgh BP, Helbing WA, Steendijk P, Schoof PH, Baan J. Biventricular systolic function in young lambs subject to chronic systemic right ventricular pressure overload. *Am J Physiol Heart Circ Physiol* 281: H2697–H2704, 2001. doi:10.1152/ajpheart.2001.281.6.H2697.
 26. Liu A, Schreier D, Tian L, Eickhoff JC, Wang Z, Hacker TA, Chesler NC. Direct and indirect protection of right ventricular function by estrogen in an experimental model of pulmonary arterial hypertension. *Am J Physiol Heart Circ Physiol* 307: H273–H283, 2014. doi:10.1152/ajpheart.00758.2013.
 27. Marin-Garcia J. Cardiac function in heart failure: the role of calcium cycling. In: *Heart Failure: Bench to Bedside*. (Contemporary Cardiology Series). Totowa, NJ: Humana, 2010, p. 2010.
 28. Marston SB, de Tombe PP. Troponin phosphorylation and myofilament Ca²⁺-sensitivity in heart failure: increased or decreased? *J Mol Cell Cardiol* 45: 603–607, 2008. doi:10.1016/j.yjmcc.2008.07.004.
 29. McLaughlin VV, Archer SL, Badesch DB, Barst RJ, Farber HW, Lindner JR, Mathier MA, McGoon MD, Park MH, Rosenson RS, Rubin LJ, Tapson VF, Varga J, Harrington RA, Anderson JL, Bates ER, Bridges CR, Eisenberg MJ, Ferrari VA, Grines CL, Hlatky MA, Jacobs AK, Kaul S, Lichtenberg RC, Lindner JR, Moliterno DJ, Mukherjee D, Pohost GM, Rosenson RS, Schofield RS, Shubrooks SJ, Stein JH, Tracy CM, Weitz HH, Wesley DJ; ACCF/AHA. ACCF/AHA 2009 expert consensus document on pulmonary hypertension: a report of the American College of Cardiology Foundation Task Force on Expert Consensus Documents and the American Heart Association: developed in collaboration with the American College of Chest Physicians, American Thoracic Society, Inc., and the Pulmonary Hypertension Association. *Circulation* 119: 2250–2294, 2009. doi:10.1161/CIRCULATIONAHA.109.192230.
 30. Mehra MR, Park MH, Landzberg MJ, Lala A, Waxman AB; International Right Heart Failure Foundation Scientific Working Group. Right heart failure: toward a common language. *J Heart Lung Transplant* 33: 123–126, 2014. doi:10.1016/j.healun.2013.10.015.
 31. Naeije R, Manes A. The right ventricle in pulmonary arterial hypertension. *Eur Respir Rev* 23: 476–487, 2014. doi:10.1183/09059180.00007414.
 32. Onodera T, Tamura T, Said S, McCune SA, Gerdes AM. Maladaptive remodeling of cardiac myocyte shape begins long before failure in hypertension. *Hypertension* 32: 753–757, 1998. doi:10.1161/01.HYP.32.4.753.
 33. Patel JR, Pleitner JM, Moss RL, Greaser ML. Magnitude of length-dependent changes in contractile properties varies with titin isoform in rat ventricles. *Am J Physiol Heart Circ Physiol* 302: H697–H708, 2012. doi:10.1152/ajpheart.00800.2011.
 34. Potus F, Ruffenach G, Dahou A, Thebault C, Breuils-Bonnet S, Tremblay É, Nadeau V, Paradis R, Graydon C, Wong R, Johnson I, Paulin R, Lajoie AC, Perron J, Charbonneau E, Joubert P, Pibarot P, Michelakis ED, Provencher S, Bonnet S. Downregulation of MicroRNA-126 contributes to the failing right ventricle in pulmonary arterial hypertension. *Circulation* 132: 932–943, 2015. doi:10.1161/CIRCULATIONAHA.115.016382.
 35. Rain S, Andersen S, Najafi A, Gammelgaard Schultz J, da Silva Gonçalves Bós D, Handoko ML, Bogaard HJ, Vonk-Noordegraaf A, Andersen A, van der Velden J, Ottenheijm CA, de Man FS. Right ventricular myocardial stiffness in experimental pulmonary arterial hypertension: relative contribution of fibrosis and myofibrillar stiffness. *Circ Heart Fail* 9: 9, 2016. doi:10.1161/CIRCHEARTFAILURE.115.002636.
 36. Rain S, Handoko ML, Trip P, Gan CT, Westerhof N, Stienen GJ, Paulus WJ, Ottenheijm CA, Marcus JT, Dorfmueller P, Guignabert C, Humbert M, Macdonald P, Dos Remedios C, Postmus PE, Saripalli C, Hidalgo CG, Granzier HL, Vonk-Noordegraaf A, van der Velden J, de Man FS. Right ventricular diastolic impairment in patients with pulmonary arterial hypertension. *Circulation* 128: 2016–2025, 2013. doi:10.1161/CIRCULATIONAHA.113.001873.
 37. Ryan JJ, Tedford RJ. Diagnosing and treating the failing right heart. *Curr Opin Cardiol* 30: 292–300, 2015. doi:10.1097/HCO.0000000000000164.
 38. Savinova OV, Gerdes AM. Myocyte changes in heart failure. *Heart Fail Clin* 8: 1–6, 2012. doi:10.1016/j.hfc.2011.08.004.
 39. Schreier D, Hacker T, Song G, Chesler N. The role of collagen synthesis in ventricular and vascular adaptation to hypoxic pulmonary hypertension. *J Biomech Eng* 135: 021018, 2013. doi:10.1115/1.4023480.
 40. Schwinger RHG, Böhm M, Koch A, Schmidt U, Morano I, Eissner HJ, Überfuhr P, Reichart B, Erdmann E. The failing human heart is unable to use the Frank-Starling mechanism. *Circ Res* 74: 959–969, 1994. doi:10.1161/01.RES.74.5.959.
 41. Tabima DM, Hacker TA, Chesler NC. Measuring right ventricular function in the normal and hypertensive mouse hearts using admittance-derived pressure-volume loops. *Am J Physiol Heart Circ Physiol* 299: H2069–H2075, 2010. doi:10.1152/ajpheart.00805.2010.
 42. Tabima DM, Philip JL, Chesler NC. Right ventricular-pulmonary vascular interactions. *Physiology (Bethesda)* 32: 346–356, 2017. doi:10.1152/physiol.00040.2016.
 43. Terui T, Sodnomtseren M, Matsuba D, Udaka J, Ishiwata S, Ohtsuki I, Kurihara S, Fukuda N. Troponin and titin coordinately regulate length-dependent activation in skinned porcine ventricular muscle. *J Gen Physiol* 131: 275–283, 2008. doi:10.1085/jgp.200709895.
 44. Tracy RE, Sander GE. Histologically measured cardiomyocyte hypertrophy correlates with body height as strongly as with body mass index. *Cardiol Res Pract* 2011: 658958, 2011. doi:10.4061/2011/658958.
 45. van der Velden J, de Jong JW, Owen VJ, Burton PBJ, Stienen GJM. Effect of protein kinase A on calcium sensitivity of force and its sarcomere length dependence in human cardiomyocytes. *Cardiovasc Res* 46: 487–495, 2000. doi:10.1016/S0008-6363(00)00050-X.
 46. van der Velden J, Papp Z, Zaremba R, Boontje NM, de Jong JW, Owen VJ, Burton PBJ, Goldmann P, Jaquet K, Stienen GJM. Increased Ca²⁺-sensitivity of the contractile apparatus in end-stage human heart failure results from altered phosphorylation of contractile proteins. *Cardiovasc Res* 57: 37–47, 2003. doi:10.1016/S0008-6363(02)00606-5.

47. Voelkel NF, Gomez-Arroyo J, Abbate A, Bogaard HJ. Mechanisms of right heart failure-A work in progress and a plea for failure prevention. *Pulm Circ* 3: 137–143, 2013. doi:10.4103/2045-8932.109957.
48. Voelkel NF, Quaife RA, Leinwand LA, Barst RJ, McGoon MD, Meldrum DR, Dupuis J, Long CS, Rubin LJ, Smart FW, Suzuki YJ, Gladwin M, Denholm EM, Gail DB; National Heart, Lung, and Blood Institute Working Group on Cellular and Molecular Mechanisms of Right Heart Failure. Right ventricular function and failure: report of a National Heart, Lung, and Blood Institute working group on cellular and molecular mechanisms of right heart failure. *Circulation* 114: 1883–1891, 2006. doi:10.1161/CIRCULATIONAHA.106.632208.
49. Walker LA, Walker JS, Glazier A, Brown DR, Stenmark KR, Buttrick PM. Biochemical and myofilament responses of the right ventricle to severe pulmonary hypertension. *Am J Physiol Heart Circ Physiol* 301: H832–H840, 2011. doi:10.1152/ajpheart.00249.2011.
50. Wang Z, Chesler NC. Pulmonary vascular wall stiffness: An important contributor to the increased right ventricular afterload with pulmonary hypertension. *Pulm Circ* 1: 212–223, 2011. doi:10.4103/2045-8932.83453.
51. Wang Z, Schreier DA, Hacker TA, Chesler NC. Progressive right ventricular functional and structural changes in a mouse model of pulmonary arterial hypertension. *Physiol Rep* 1: e00184, 2013. doi:10.1002/phy2.184.
52. Weil J, Eschenhagen T, Hirt S, Magnussen O, Mittmann C, Remmers U, Scholz H. Preserved Frank-Starling mechanism in human end stage heart failure. *Cardiovasc Res* 37: 541–548, 1998. doi:10.1016/S0008-6363(97)00227-7.
53. Wu Y, Cazorla O, Labeit D, Labeit S, Granzier H. Changes in titin and collagen underlie diastolic stiffness diversity of cardiac muscle. *J Mol Cell Cardiol* 32: 2151–2162, 2000. doi:10.1006/jmcc.2000.1281.
54. Xu J, Nagata K, Obata K, Ichihara S, Izawa H, Noda A, Nagasaka T, Iwase M, Naoe T, Murohara T, Yokota M. Nicorandil promotes myocardial capillary and arteriolar growth in the failing heart of Dahl salt-sensitive hypertensive rats. *Hypertension* 46: 719–724, 2005. doi:10.1161/01.HYP.0000185189.46698.15.
55. Zimmer HG, Gerdes AM, Lortet S, Mall G. Changes in heart function and cardiac cell size in rats with chronic myocardial infarction. *J Mol Cell Cardiol* 22: 1231–1243, 1990. doi:10.1016/0022-2828(90)90060-F.
56. Zuo HJ, Liu ZX, Liu XC, Yang J, Liu T, Wen S, Wang DW, Zhang X. Assessment of myocardial blood perfusion improved by CD151 in a pig myocardial infarction model. *Acta Pharmacol Sin* 30: 70–77, 2009. doi:10.1038/aps.2008.10.

